Shrinkage Force Studies of Oriented Polyethylene Terephthalate

S. D. LONG and I. M. WARD*

IRC in Polymer Science and Technology, University of Leeds, Leeds, LS2 9JT, UK

SYNOPSIS

Shrinkage force measurements on drawn polyethylene terephthalate fibres have been evaluated in terms of the elastic behaviour of a molecular network. It is shown that for low network deformations the classical theory of Kuhn and Grün describes the stress-optical behaviour very well. For high deformations, the recent theory of Edwards and Vilgis has been found to give a satisfactory description of the data. It also provides some tentative insights into the structure of the spun yarns.

INTRODUCTION

This article concerns the development of shrinkage force and free shrinkage in PET fibres when raised above their glass transition temperature. It relates to a separate publication[1] describing the drawing behaviour and properties of a wide range of fibres prepared by melt spinning over a wide range of wind-up speeds (WUS). A particular feature of this latter publication is the use of the network draw ratio, obtained by matching the stress–strain curves of the drawn yarns.

The earliest investigation of the stress-optical properties of PET was conducted by Pinnock and Ward,[2] who found the free shrinkage of amorphous as-spun PET fibres to relate to both the birefringence and the peak shrinkage stress. The stress-optical behaviour was quantitatively analysed in terms of the classical Kuhn and Grün theory[3] for a stretched rubber network. A particular feature of this work was the use of free shrinkage as a measure of overall network extension in the low WUS amorphous yarns. It was difficult to obtain an accurate measure of overall network extension unless the free shrinkage measurements were carried out over a range of temperatures.

It has since become clear that crystallinity will develop, either as a result of increasing WUS or hot draw ratio, and lead to a fall in shrinkage at higher orientation. Thus, free shrinkage can no longer relate to overall network extension.

The difficulty in relating free shrinkage to the network extension leads to the use of the geometric hot draw ratio resulting from hot drawing in the analysis of shrinkage force data by Rietsch et al.[4] The retractive force was found to relate to draw ratio according to the Gaussian theory [see eq. (1) below] for $\lambda \leq 1.7$, i.e., before crystallisation occurs in drawing.

Bhatt and Bell[5] used the Treloar[3] modification of the Kuhn–Grün theory to model the full extension range. If the number of statistical segments is constant (as is conventional), this equation does not appear to model the development of amorphous orientation with extension very successfully.

In the present investigation, the geometric hot draw ratio λ_{hd} does not relate to the network extension because of the different initial extensions imposed in the spinline. However, the birefringence correlates well with the total network draw ratio λ_{net} up to λ_{net} of 3.5. As λ_{net} rises above this value, differences develop between the pin-drawn yarns, which are dependent on feedstock WUS. However, in view of the good agreement between birefringence and λ_{net} at low and intermediate strains, the network draw ratio has been combined with peak shrinkage force measurements to define the stress–extension ratio relationship. In this way, the shrinkage force results for oriented semi-crystalline PET yarns can be analysed in the situation where crystallisation

* To whom correspondence should be addressed.

Journal of Applied Polymer Science, Vol. 42, 1921–1929 (1991)
 CCC 0021-8995/91/071921-09$04.00

prevents any accurate measure of the deformation to be obtained from shrinkage measurements.

The previous studies[2,4,5] have also based the interpretation on classical rubber network elasticity theory, which does not seem appropriate for crystalline materials. The recent sliplink theory of Edwards and Vilgis[6] aims to describe the situation where there are both permanent crosslinks (in this case the crystallites) and physical entanglements (the sliplinks). As it also models the whole of the rubberlike stress–strain curve, it was considered appropriate to examine the application of this theory to PET fibres.

THEORY

Classical Rubber Elasticity

Classical rubber elasticity theory can be used to relate the peak shrinkage stress in an amorphous fibre to the extension ratio λ

$$t = NkT(\lambda^2 - \lambda^{-1}), \tag{1}$$

where t is the peak shrinkage force per unit deformed cross-sectional area, k the Boltzmann constant, T the absolute temperature, and N the classical entanglement density.

Equation (1) can be modified to give the molecular weight between network junction points M_c,

$$t = \frac{\rho RT}{M_c}(\lambda^2 - \lambda^{-1}), \tag{2}$$

where ρ is the density and R the gas constant.

Kuhn and Grün obtained the following expression for the optical anisotropy of the Gaussian network[3]:

$$\Delta n = \frac{2\pi}{45}\frac{(\mathbf{n}^2 + 2)^2}{\mathbf{n}} N(\alpha_1 - \alpha_2)(\lambda^2 - \lambda^{-1}), \tag{3}$$

where $\mathbf{n}$ is the mean refractive index (found to be 1.58 for PET) and $(\alpha_1 - \alpha_2)$ the polarizability of the random link.

Combining eqs. (1) and (3), a stress-optical coefficient can be found:

$$C = \frac{\Delta n}{t} = \frac{2\pi}{45}\frac{(\mathbf{n}^2 + 2)^2}{\mathbf{n}kT}(\alpha_1 - \alpha_2), \tag{4}$$

which is independent of the extension. The polarazability difference of the random link can therefore be found directly from the stress-optical behaviour.

The work of Pinnock and Ward[2] replaces the λ term in the above equations by $(1 - S)^{-1}$ where S is the free shrinkage. Thus, eq. (3) can be rewritten as

$$\Delta n = \frac{2\pi}{45}\frac{(\mathbf{n}^2 + 2)^2}{\mathbf{n}} N(\alpha_1 - \alpha_2) \times [(1 - S)^{-2} - (1 - S)]. \tag{5}$$

Whilst the peak shrinkage stress is relatively constant over a range of temperature,[2,4,7] the free shrinkage is highly sensitive.[2]

Mooney–Rivlin Equation

As the draw ratio of the originally amorphous polymer rises above 1.5, the experimental results fall below that predicted by eq. (1).[3,4] This feature is known as strain-softening and can be modelled by the Mooney–Rivlin equation[8,9]:

$$s = (\lambda - \lambda^{-2})(C_1 + C_2/\lambda), \tag{6}$$

where s is the nominal shrinkage stress, and is related to the true shrinkage stress by

$$t = s\lambda.$$

C_1 and C_2 are empirical constants. Rearranging eq. (6) gives

$$s^* = \frac{s}{(\lambda - \lambda^{-2})} = C_1 + C_2/\lambda, \tag{7}$$

where s^* is the reduced force. A Mooney–Rivlin plot shows s^* as a function of λ^{-1}.

Work on vulcanized rubbers has shown C_1 to be dependent on the degree of chemical crosslinking and C_2 to be relatively independent.[10,11] C_1 has been found to be independent of sovlent uptake whilst C_2 falls progressively[11] and may be a function of the effectiveness of molecular entanglements. However, the Mooney–Rivlin theory has no molecular basis and is generally considered to be unsatisfactory.

Edwards–Vilgis Theory

More recent work by S. F. Edwards and coworkers[6] has considered the effect of molecular entanglements and finite chain extensibility on the elasticity of crosslinked networks. These entanglements are modelled as sliplinks that are effectively a development of the well-established reptation concept.

Edwards and Vilgis derive the following expression for the free energy of the network[6]

$$\frac{F}{kT} = \frac{1}{2} N_c \left[\frac{\sum(1-\alpha^2)\lambda_i^2}{1-\alpha^2 \sum \lambda_i^2} + \ln(1-\alpha^2 \sum \lambda_i^2) \right] + \frac{1}{2} N_s \sum \left[\frac{\lambda_i^2(1+\eta)(1-\alpha^2) + \ln(1+\eta\lambda_i^2)}{(1+\eta\lambda_i^2)(1-\alpha^2\lambda_i^2)} + \ln(1-\alpha^2\lambda_i^2) \right], \quad (8)$$

where N_c and N_s are the densities of permanent and temporary entanglements, respectively, α is an inextensibility parameter, and η is a measure of the mobility of the temporary entanglements (sliplinks). The theoretical maximum draw ratio is given by

$$\lambda_{max} = \alpha^{-1}. \quad (9)$$

If $\eta = 0$, the sliplinks are fixed and will behave as permanent entanglements. An argument minimizing F leads to a value of $\eta = 0.2343$, which corresponds to each link being able to slide on average as far as the centre of its topologically neighbouring link.[12] In the case of uniaxial extension, the constant volume condition is used:

$$\sum_1^3 \lambda_i^2 = \lambda_3^2 + \frac{2}{\lambda_3}, \quad (10)$$

where λ_3 is the extensional draw ratio, and the force is calculated from

$$s = \left(\frac{\partial F}{\partial \lambda} \right)_T.$$

EXPERIMENTAL

Sample Preparation

The feedstock spun yarns were produced by melt spinning at 292°C and wound up at eight speeds in the range 0.46–4.5 km/min. Further details of these spun yarns, referred to as A, B, etc., are given in Table I. The spun yarns A, B, C, E, F, and H were drawn over a heated roller (the pin) at 85°C to produce a series of drawn yarns for the shrinkage force measurements. It is important to note that there is appreciable crystallisation occurring at the spinning stage in the case of yarns F and H.

Table I Details of Spun Yarns

Yarn	WUS (km/min)	T_s (°C)	Δn × 1000	d (mm)
A	0.5	292	2.6	44.8
B	0.9	292	5.7	41.0
C	1.5	292	10.7	37.5
D	2.1	292	19.3	32.1
E	3.0	292	40.8	28.6
F	3.7	292	61.8	27.1
H	4.6	292	95.3	24.8

WUS, wind-up speed; T_s, spinning temperature; Δn birefringence; d, diameter.

Measurement of the Network Draw Ratio

The network draw ratio for each sample was determined by matching the true stress–strain curves of each drawn yarn with the lowest WUS precursor. The procedure follows that originally advocated by Brody[13] and described in detail in the previous publication.[1]

Shrinkage Force

The apparatus used has been previously described by Capaccio and Ward.[14] In summary, the test involves clamping a 6.5 cm length of yarn between two grips that are then lowered into a silicone oil bath maintained at 88°C. The retractive force that develops is transmitted to a strain gauge transducer and output saved on a chart recorder (Fig. 1).

Work by Perena et al.[7] revealed the presence of a second maximum in the shrinkage force that arose in oriented samples some time after the peak shrinkage stress and was attributed to crystallisation. This second peak has been observed during this study and as the sample orientation rises the separation of the two maxima is reduced.

Free Shrinkage

A 2 m length of yarn was immersed in hot silicone oil at 100°C for 2 min. The yarn was then removed and the new sample length measured. The percentage shrinkage was calculated using

$$S = \frac{(l_0 - l_1)}{l_0} \times 100, \quad (11)$$

where l_0 and l_1 are the original and shrunken sample lengths, respectively.

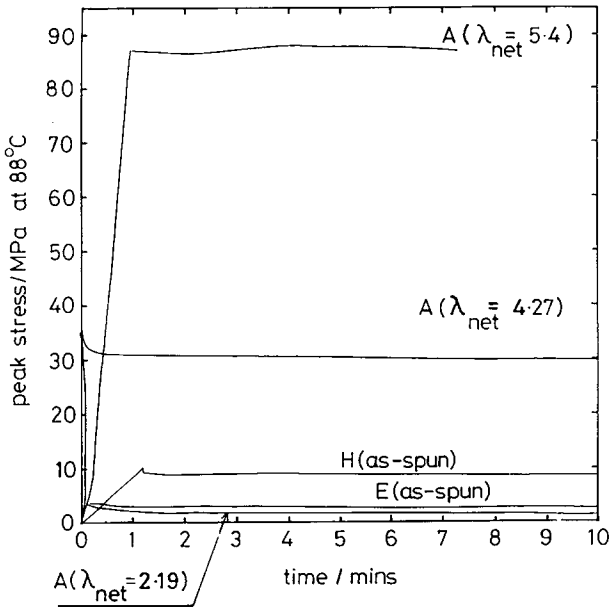

Figure 1 Shrinkage stress t as a function of time.

Silicone oil was used as the heating medium for both the free shrinkage and shrinkage force measurements because of the reported plasticizing effect of water on PET.[2]

Fitting Procedure

Each spun yarn was considered a unique state that was subsequently extended in the drawing process. This unique network had developed by the spinline orientation process as winding speed increased.[1] The overall extension route of a particular spun yarn includes both the extension of the melt-spun network in the spinline up to the WUS of the yarn being considered and the hot drawing of that yarn. This will be illustrated by Mooney–Rivlin plots for the fitted networks.

The Mooney–Rivlin coefficients C_1 and C_2 were found to be 73 kPa and 0.94 MPa, using results from all spun and drawn yarns. In the light of earlier work,[10,11] it seemed that C_1 could be related to the crosslink density and C_2 is a function of the effectiveness of physical entanglements. Thus, the following were used as starting values in the initial fit:

$$N_c = \frac{C_1}{kT} \quad \text{and} \quad N_s = \frac{C_2}{kT}.$$

The procedure used is similar to that described by Brereton and Klein,[15] in which inputted values of nominal peak shrinkage stress and λ_{net} are fitted to the expression of Thirion and Weil[16]:

$$s^* = kT[N_c + N_s H(\eta, \lambda)] \qquad (12a)$$

and $H(\eta, \lambda)$ is given by

$$H(\eta, \lambda) = \frac{\lambda^2}{\lambda^2 + \lambda + 1} \times \left[\frac{1}{(\lambda + \eta)^2} + \frac{\lambda + 1}{\lambda(1+\eta\lambda^2)^2}\right]. \qquad (12b)$$

The work hardening that occurs at high strains was excluded from this initial fit. In the fitting procedure and all other calculations presented here, we have used the network draw ratio as a measure of overall network extension, i.e., it has to be assumed that

$$\lambda_{net} \equiv \lambda$$

for all previous equations. (**Note:** Strictly C_2 should relate to both the density of slip links (N_c) and the mobility of the links (η).)

A further program attempted to fit the whole deformation range by introducing the inextensibility α. In an iterative process, the program adjusted the parameters N_c, N_s, α, and η to minimise the deviation. However, results showed that there was a fall in reduced force s^* at very high λ_{net} that the Edwards–Vilgis theory is unable to accommodate. Data from this region ($\lambda_{net} > 4.6$) was excluded from the fits. This fall has tentatively been associated with

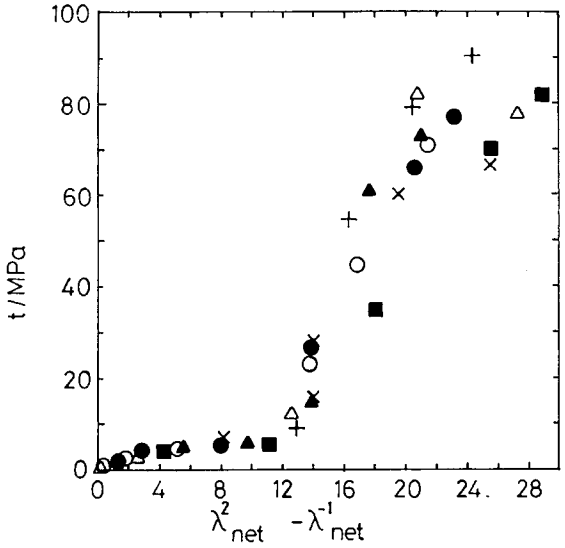

Figure 2 Shrinkage stress t vs. $\lambda_{net}^2 - \lambda_{net}^{-1}$ for precursors and pin-drawn yarns. ■, A; ○, B; ●, C; △, D; ▲, E; ×, F; +, H.

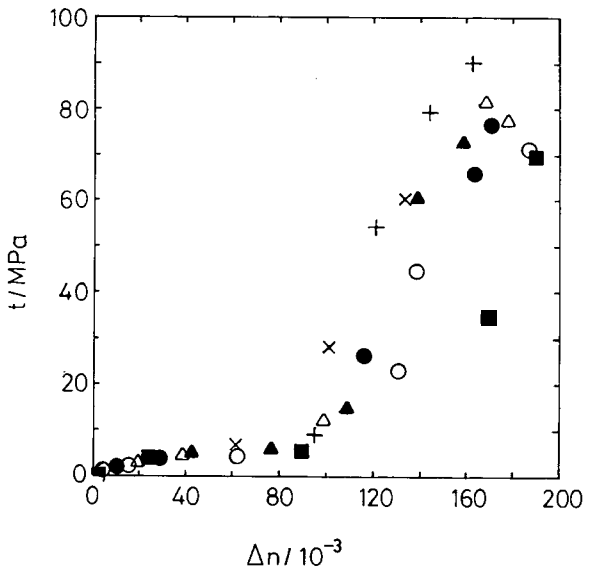

Figure 3 Shrinkage stress t vs. birefringence Δn (symbols as in Fig. 2).

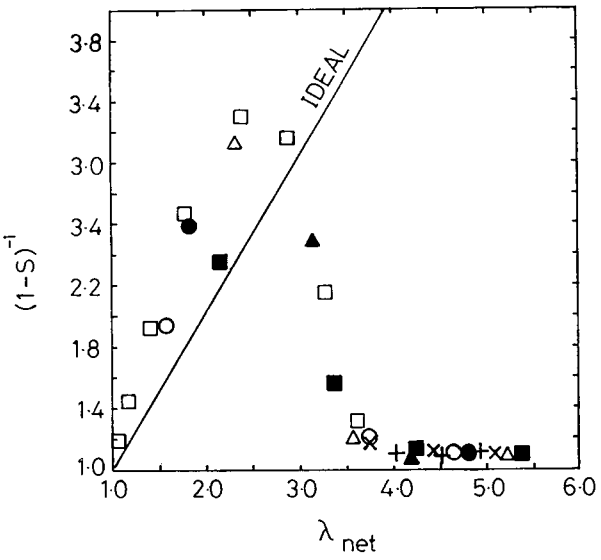

Figure 5 Free shrinkage vs. network draw ratio λ_{net}. "Ideal" line represents $(1-s)^{-1} = \lambda_{net}$. □, as spun (other symbols as in Fig. 2).

crystallisation, which may affect the development of retractive force in the amorphous phase.

Results and Discussion

Figure 2 shows the development of peak shrinkage stress with increasing λ_{net} and eq. (1) is valid for $\lambda_{net} \leq 1.8$. Above this value, the expected strain softening is observed. The results for both the precursor and pin-drawn yarns lie about a common path until strain hardening occurs at $\lambda_{net} > 3.5$, i.e., $(\lambda^2 - \lambda^{-1}) \sim 12$. In this region, there is a clear rise in the rate of work-hardening with precursor WUS and as λ_{net} rises further there is a levelling off in the stress and for some drawn yarn networks a fall is seen.

Figure 3 is similar in pattern to Figure 2. At low orientation, there is a constant stress-optical coefficient as predicted by the Kuhn–Grün theory, but deviation develops as birefringence rises above

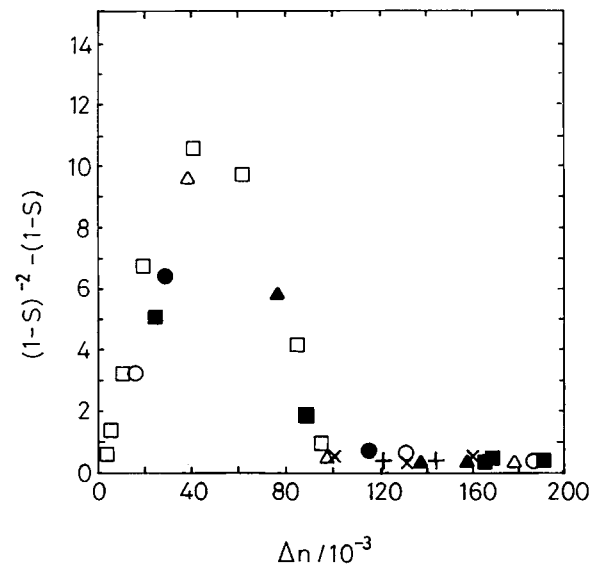

Figure 4 Free shrinkage s vs. birefringence Δn. □, as spun (other symbols as in Fig. 2).

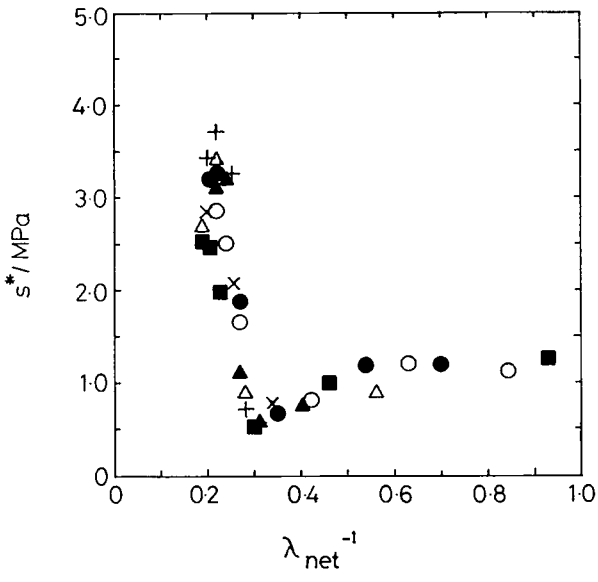

Figure 6 $s^* = s/\lambda_{net} - \lambda_{net}^{-2}$ vs. λ_{net}^{-1}, where s = nominal shrinkage stress (symbols as in Fig. 2).

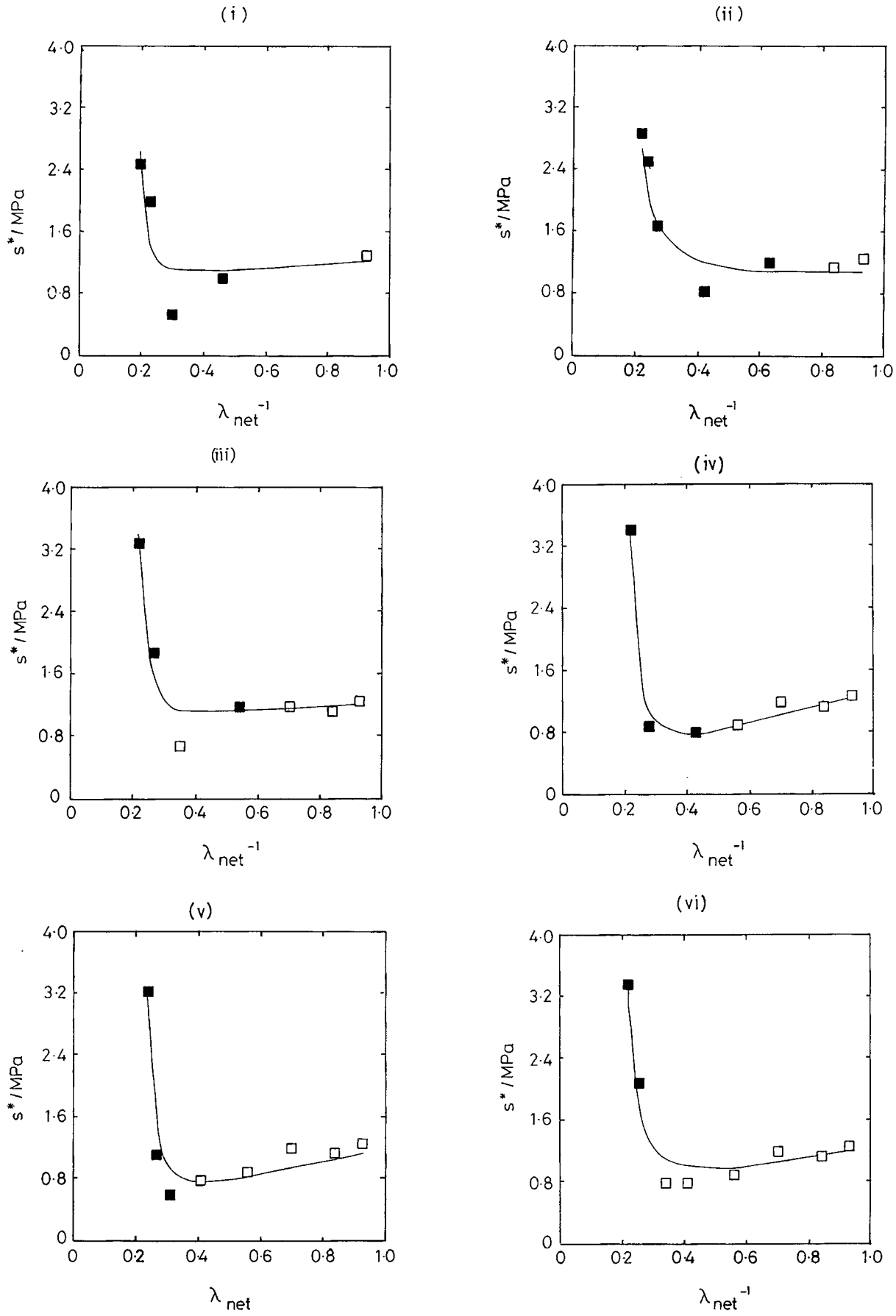

Figure 7

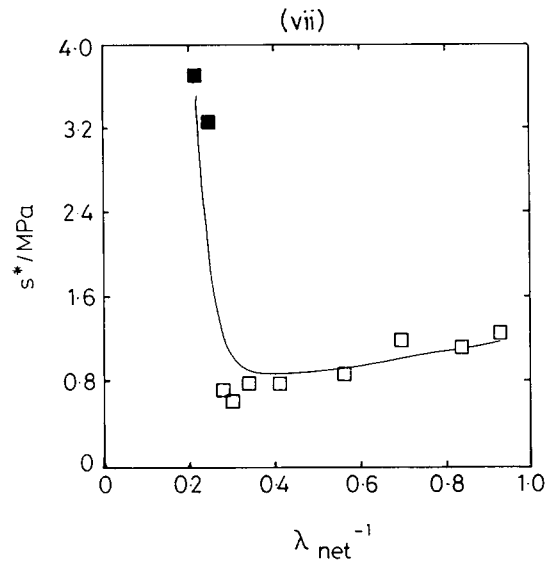

Figure 7 Fits of experimental data to Edwards–Vilgis theory. □, spun precursors; ■, pin-drawn yarns; —, fitted line. Figures denoted as (i), (ii), (iii) ... (vii) show fits for series, *A*, *B*, *C*, *D*, *E*, *F*, and *H*.

0.025 and a separation of drawing response only arises at $\Delta n > 0.095$ when the drawn yarns again fall onto curves determined by precursor WUS.

Considering these results and those of Ward et al.,[2,4,7] there is clear support for the existence of a classical rubberlike network in PET at low levels of molecular orientation. It was assumed in the previous work that physical entanglements act like permanent crosslinks and there was no consideration of mobile entanglements or sliplinks.

From eq. (1) it was found that the classical entanglement density N was 2.63×10^{26} m^{-3}, which corresponds to a molecular weight between network junction points of 3,070 g mol^{-1}. The good agreement with classical theory at $\lambda_{net} \leq 1.8$ shows that the spinning and pin-drawing processes involve the affine deformation of an entanglement-based network.

Analysis of Figure 3 using the stress-optical theory results in a value for the polarizability of the random link of 1.67×10^{29} m^{-3}, in good agreement with published values.[1,4] It is significant that the theory correctly predicts that the stress-optical constant is independent of variation in N.

Figure 4 shows that eq. (5) holds up to a birefringence of 0.020 although there is a slight separation between the precursors and the drawn yarns. As Δn increases, the shrinkages fall below the linear relationships, and following the maximum at $\Delta n = 0.040$ there is a sharp fall to very low shrinkages. N was calculated using eq. (5) and was found to be 0.89×10^{26} m^{-3}, which is three times lower than that obtained from the variation of peak shrinkage stress with λ_{net}.

In eq. (5) it was assumed that the $\lambda_{net} = (1 - S)^{-1}$, but Figure 5 shows that even at low λ_{net}, when crystallinity has not intervened, the shrinkages are greater than expected, leading to the lower value of N. The reason for the shrinkage being greater than expected is not immediately apparent. At low orientation, free shrinkage does not result in the negative birefringences reported by Pinnock and Ward,[2] precursors *A* to *E* retracting to the isotropic state. However, in a real network there will be a range of entanglement separations (**R**) and when heated to the rubberlike state the shortest chains in the extended network will disorder first. This corresponds to the peak shrinkage stress shown in Figure 1. At this stage, the longer network chains are not fully disordered and shrinkage continues until no further reduction in free energy is possible (for these low orientation amorphous yarns, possible crystallisation effects have been neglected). Although free shrinkage is initially rapid, it is known to continue to increase with time.[2]

The peak shrinkage force is due to the retraction of the shortest chains and it is these chains that are thought to control the load-bearing properties, particularly tensile modulus.[1] Free shrinkage, on the other hand, is due to the disordering of all the chains in the "biased" network. The small differences between the low orientation precursor and pin-drawn yarns indicate a broader distribution of **R** in the as-spun material.

Figures 2 and 3 have revealed that differences only develop between the precursor yarn networks in the work-hardening region. The sliplink model of Edwards and Vilgis has been used to investigate differences between these networks.

The Mooney–Rivlin plot (Fig. 6) represents the Gaussian region by a line of zero slope. As λ_{net} rises above 1.8, strain-softening is observed, followed by the typical sharp upturn in the reduced force s^* due to work-hardening. There is, however, an unexpected fall in s^* at $\lambda_{net} \geq 4.6$ for networks *C*, *D*, *E*, *F*, and *H* and a possible levelling-off for networks *A* and *B*. This fall may be due to crystallization, which will produce a significant amount of extended chain crystals in the high-WUS networks. These crystals may act as a link between other crystallites and hinder shrinkage.

Figure 7 shows the Edward–Vilgis theory fits to the individual networks. Overall, this theory, which does not consider the Gaussian region by assuming that there is no barrier to the motion of the slip-

links, provides a reasonable fit in the range $4.6 < \lambda_{net} < 1.8$.

It is useful to consider the individual fits in some detail. Yarn drawn from feedstock A initially obeys the classical theory and as λ_{net} rises there is pronounced strain-softening followed by the characteristic upturn. The fit to this network is relatively poor given the sharp change in slope following the Gaussian region.

As the precursor orientation rises, there is a decrease in the gradient of the srain-softening region and an improvement in the quality of the fits, although at the highest WUS (network H) the upturn due to strain-hardening does not seem to be modelled especially well. These fits, which have included the low λ_{net} data, are thus a compromise between the classical network theory and the sliplink-based description of strain-softening.

The sliplink theory, which allows the molecular entanglements to be mobile at low strains, has not considered the successful application of classical theory to noncrosslinked systems in which the entanglements are fixed at low λ_{net}. The fitted values of N_s shown in Table II are of the same order as N [from eq. (1)], supporting the proposal that the classical network is entanglement based. Strain-softening behaviour is well modelled by the Edwards–Vilgis theory and arises when the entanglements overcome an energy barrier. There is thus a flow stress associated with the motion of the sliplinks. The sliplink theory, in common with other rubber elasticity models, does not consider the effect of internal energy changes. In PET, this internal energy effect is apparent even at relatively low strains in a change from the gauche to trans conformation of the ethylene glycol residue.

The fitted parameters are given in Table II. They show that, as expected, the networks are dominated by sliplinks that are very stiff for the low-WUS networks (A, B, and C). As the feedstock orientation rises further, there is a rise in N_s and in the mobility parameter η. Thus, network D, E, F, and H contain more sliplinks but conversely these links are more mobile. Significantly, the results show a very low value of N_c except for the highest orientation networks F and H, where the influence of spin-line crystallization is apparent. However, it is worth recalling that the greatest strain-softening was observed for the low-WUS networks and these fits are less reliable than for the high-WUS networks.

Table II Characterization of the Entangled Molecular Networks

Network	N_c	N_s	η	α	λ_{max}	λ_t
A	0.08	2.27	0.06	0.151	6.63	6.32
B	0.08	1.86	0.01	0.147	6.80	5.91
C	0.02	2.28	0.07	0.175	5.72	5.92
D	0.00	3.37	0.32	0.184	5.43	5.88
E	0.00	3.06	0.35	0.198	5.06	6.17
F	0.61	3.31	0.62	0.176	5.68	5.96
H	0.31	2.48	0.26	0.182	5.49	5.99

λ_t is the experimental maximum draw ratio and λ_{max} is the theoretical maximum found from the fit. N_c and N_s are given in units of 10^{26} m^{-3}.

The gradual rise in η is of importance since it may relate to a decrease in amorphous region orientation that accompanies crystallization during spinning and drawing. This may reflect the increasingly biased nature of the pin-drawn networks as WUS rises, as discussed previously.[1]

The experimental maximum draw ratio λ_t is relatively constant at about 6.0 and with the exception of networks A and B, the predicted values (λ_{max}) are lower and more variable. The theory is not able to provide precise values of maximum extensibility since it does not model the very high λ_{net} falloff in reduced force.

CONCLUSIONS

In light of this study and earlier investigations of the rubberlike behaviour of PET, it is clear that the classical network is due to the effect of molecular entanglements that are immobile at $\lambda_{net} \leq 1.8$. These entanglements have an energy barrier associated with their motion that is related to conformational changes within the ethylene glycol residue. The Edwards–Vilgis theory does not accommodate this and other internal energy effects, such as crystallization, and is unable to model the classical region.

The Edwards–Vilgis theory is able to model the data well in the range $4.6 < \lambda_{net} < 1.8$. As λ_{net} rises above 4.6, there is a clear drop in reduced shrinkage force that the theory cannot accommodate. This high λ_{net} deviation may be due to the crystallinity becoming continuous and hindering the development of shrinkage force.

In conclusion, the rubberlike elasticity of PET can be considered in terms of two regimes: the low-strain Gaussian region, and following the strain-induced activation of the sliplinks the Edward–Vilgis provides a good description for $\lambda_{net} < 4.6$.

The discrepancy between estimated values of the classical entanglement density is due to the differing origins of shrinkage force and free shrinkage. Peak

shrinkage force has been associated with the mechanically important shortest chains, whilst free shrinkage is due to the disordering of all chains in the biased network.

We thank our colleagues at Leeds University for their advice and assistance, especially Dr. P. G. Klein, Dr. H. Brody, and Mr. D. L. M. Cansfield. We are also indebted to Hoechst-Celanese Fibers Division, Charlotte, NC, for support of the research project and Dr. W. Bessey for many useful discussions and for the preparation of the spun yarn samples.

REFERENCES

1. S. D. Long and I. M. Ward, *J. Appl. Polym. Sci.*, **42,** 1911 (1991).
2. P. R. Pinnock and I. M. Ward, *Trans. Farad. Soc.* **62,** 1038 (1966).
3. L. R. G. Treloar, *Physics of Rubber Elasticity,* 3rd ed., Clarendon Press (1975).
4. F. Rietsch, R. A. Duckett, and I. M. Ward, *Polymer* **20,** 1133 (1979).
5. G. M. Bhatt and J. P. Bell, *J. Polym. Sci., Polym. Phys. Ed.* **14,** 575 (1976).
6. S. F. Edwards and Th. Viligis, *Polymer* **27,** 483 (1986).
7. J. M. Perena, R. A. Duckett, and I. M. Ward, *J. Appl. Polym. Sci.* **25,** 1381 (1980).
8. M. Mooney, *J. Appl. Phys.* **11,** 582 (1940).
9. R. S. Rivlin, *J. Appl. Phys.* **18,** 444 (1948).
10. S. Gumbrell, L. Mullins, and R. S. Rivlin, *Trans. Farad. Soc.* **49,** 1495 (1953).
11. G. Allen, M. Kirkham, J. Padget, and C. Price, *Trans. Farad. Soc.* **67,** 1278 (1971).
12. R. C. Ball, M. Doi, S. F. Edwards, and M. Warner, *Polymer* **22,** 1010 (1981).
13. H. Brody, *J. Macromol. Sci. Phys.* **B22**(3), 407 (1983).
14. G. Capaccio and I. M. Ward, *Coll. Polym. Sci.* **260,** 46 (1982).
15. G. Brereton and P. G. Klein, *Polymer* **29,** 970 (1988).
16. P. Thirion and T. Weil, *Polymer* **25,** 609 (1984).

Received March 12, 1990
Accepted July 9, 1990